

Liquid crystalline behavior of tetraaryl derivatives of benzo[*c*]cinnoline, tetraazapyrene, phenanthrene, and pyrene: the effect of heteroatom and substitution pattern on phase stability†‡

Monika J. Sienkowska,§^a John M. Farrar,¶^a Fan Zhang,||^b Sharat Kusuma,^a Paul A. Heiney^b and Piotr Kaszynski*^a

Received 26th October 2006, Accepted 11th December 2006

First published as an Advance Article on the web 15th January 2007

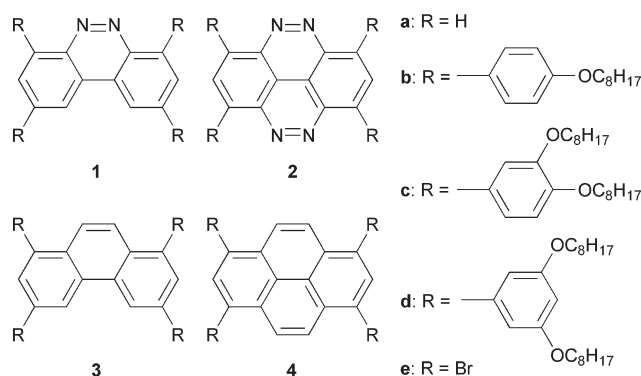
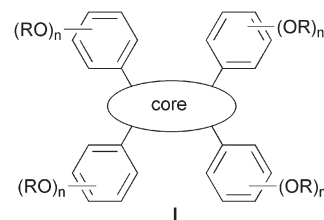
DOI: 10.1039/b615545f

A series of closely related tetrasubstituted derivatives of benzo[*c*]cinnoline (**1**), tetraazapyrene (**2**), phenanthrene (**3**), and pyrene (**4**) were investigated for their mesogenic properties using thermal, optical, spectroscopic, and powder XRD analyses. Only three 3,4-dioctyloxyphenyl derivatives exhibited mesogenic properties. Substitution of N for CH (**3** → **1** and **4** → **2** pairs) and also increase of the core element size (**1** → **2** and **3** → **4** pairs) significantly increases the mesophase stability. The findings and observed trends were rationalized by analysis of conformational properties which included calculation of the planarization energy, and modeling of aliphatic chain density and fill fractions. MO calculations showed that the tetraaza derivative **2c** is significantly electron deficient and suitable for electron conductive materials.

Introduction

Over the past decade, discotic liquid crystals^{2,3} have been recognized⁴ as potential materials for energy harvesting,⁵ light emitting diodes,^{6,7} and organic electronics.⁸ All these applications involve charge transport in the bulk phase, and for this reason the phase structure, electronic properties of the aromatic core, and the molecular packing are particularly relevant to the material's performance. Discotics with electron-rich cores are relatively numerous and many show facile hole transport properties.⁹ On the other hand, there are relatively few π -deficient discotic mesogens suitable for efficient electron transport. The majority of them are based on nitrogen-containing polycyclic heteroaromatics such as tricycloquinazoline,^{10,11} hexaazatriphenylene,^{12–14} and hexaazatrinaphthylene.^{15–17} It can be expected that other heterocycles such as benzo[*c*]cinnoline (**1a**) and 4,5,9,10-tetraazapyrene (**2a**) are also suitable structural elements for n-type organic semiconductors. Moreover, these two heterocycles provide convenient models for our design of discotic radicals in which the –N=N– group is a substitute for the spin-bearing thioaminy group.^{18,19}

In this context, we designed a class of compounds of structure **I** in which the parent heterocycles, **1a** and **2a**, are substituted by four phenyl groups bearing flexible alkoxy substituents to promote mesogenic behavior. For the purpose of the present investigations, the octyl group was selected as an alkyl chain. Derivatives **1** and **2** provide a rare opportunity for comparison of discogenic properties of heterocyclic systems with their carbocyclic analogs. Therefore, derivatives of phenanthrene (**3a**) and pyrene (**4a**) were also included in the studies.



^aOrganic Materials Research Group, Department of Chemistry, Vanderbilt University, Nashville, TN, 37235, USA

^bDepartment of Physics and Astronomy, University of Pennsylvania, Philadelphia, PA, 19104, USA

† This work has been described in part previously; see ref. 1.

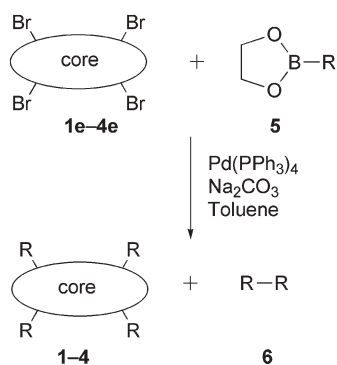
‡ Electronic supplementary information (ESI) available: XRD, DSC, synthetic and computational details including archives for the MP2/6-31G(d) results, colour photomicrographs, and literature redox data. See DOI: 10.1039/b615545f

§ Current address: University of Pennsylvania, Philadelphia, PA 19104, USA.

¶ Current address: Abraham Baldwin Agricultural College, Tifton, GA 31793, USA.

|| Current address: Argonne National Laboratory, Argonne, IL 60439, USA.

Here we report detailed studies of the influence of the number and distribution of the octyloxy chains on the solid and mesogenic properties in series **1–4**. We also analyze the effect of a replacement of the bridging –N=N– group in



Scheme 1

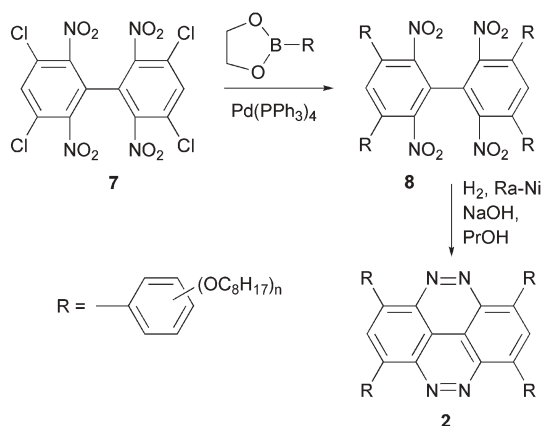
heterocycles **1** and **2** with the $-\text{CH}=\text{CH}-$ group in hydrocarbons **3** and **4** on the stability of liquid crystalline phases.

Results

Synthesis

Tetraarylarenes. Tetraarylarenes **1–4** were prepared from the corresponding tetrabromoarenes **1e–4e** and appropriate boronic esters **5** using the general Suzuki coupling procedure²⁰ (Scheme 1). Yields of the coupling products were improved by using DME as a solvent instead of toluene. In each reaction, biphenyls **6** were obtained as byproducts in the homocoupling reaction of boronic esters **5**.

Most reactions were completed overnight. Coupling reactions using the crude 1,3,6,8-tetrabromo-4,5,9,10-tetraazapyrene (**2e**) yielded tetraarylarenes **2b–2d** in yields below 3%. Therefore, an alternative method was developed for the preparation of these derivatives (Scheme 2), based on the reported preparation of the parent tetraazapyrene **2a**.²¹ Thus, the Suzuki coupling reaction of tetrachloride **7** and appropriate boronic ester **5** gave tetraaryl biphenyl **8**, which was easily purified by column chromatography. The two azo bridges were closed by the reduction²¹ of **8** with freshly prepared Raney nickel under basic conditions to give tetraazapyrenes **2b–2d**. The literature procedure was modified by using 1-propanol instead of ethanol, to increase the solubility



Scheme 2

of biphenyls **8**. The overall yields for tetraazapyrenes **2b–2d** were higher than those in the first method and ranged from 20% to 29%. Thus, the overall synthesis of **2** was significantly improved in the second method by the ease of the reaction monitoring, purification of products and their intermediates, and generally higher yields.

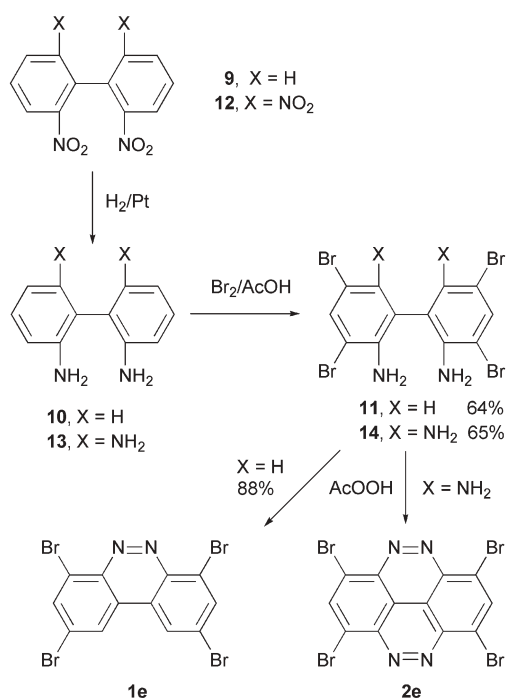
All products **1–4** were purified by gradient column chromatography using a hexanes– CH_2Cl_2 mixture as eluent. However, the chromatographic purification of tetraazapyrene derivatives **2** was not trivial, due to a number of side products formed during the reduction, and the apparently low stability of tetraazapyrene derivatives on silica gel. Chromatographic purification was followed by recrystallization, typically from hexane, ethanol–toluene, or 1-propanol except for **1d**, which appeared to be a liquid at room temperature.

Unfortunately, 1,3,6,8-tetrakis(3,5-dioctyloxyphenyl)phenanthrene (**3d**) could not be obtained in the pure form. According to the NMR analysis, **3d** was obtained as an oily mixture of several species and could not be separated either by chromatography or by recrystallization. However, based on trends in thermal behavior of other derivatives in the series (*vide infra*), it was concluded that **3d** would most likely not exhibit liquid crystalline behavior, and it was not pursued further.

The purity of all tetraarylated arenes **1–4** was confirmed by normal phase analytical HPLC, with a hexane– CH_2Cl_2 mixture as an eluent.

Tetrahaloarenes. 1,3,6,8-Tetrabromobenzo[*c*]cinnoline²² (**1e**, Scheme 3), was synthesized according to a modified literature method. Catalytic reduction of 2,2'-dinitrobiphenyl²³ (**9**) followed by bromination of the resulting 2,2'-diaminobiphenyl (**10**) in a mixture of acetic and hydrochloric acids gave the tetrabromo derivative **11** in 64% overall yield. The diamine **11** was oxidized with peracetic acid to form **1e** in 88% yield.²²

The synthesis of 1,3,6,8-tetrabromo-4,5,9,10-tetraazapyrene (**2e**, Scheme 3) was attempted in a similar way to the preparation of **1e** starting from 2,2',6,6'-tetranitrobiphenyl²¹ (**12**), which was prepared in the Ullmann coupling of 2,6-dinitrochlorobenzene. Catalytic reduction of **12** gave tetraamine²¹ **13** as a dark red solid in 88%–90% yield. Without further purification, 2,2',6,6'-tetraaminobiphenyl (**13**) was brominated in a mixture of acetic and hydrochloric acids to yield 61%–66% of 2,2',6,6'-tetraamino-3,3',5,5'-tetrabromobiphenyl (**14**). The product was purified chromatographically with CH_2Cl_2 as an eluent. The subsequent closure of the azo bridges by peracetic acid oxidation was not trivial. A brownish suspension of tetraamine **14** in acetic acid turned black after the addition of peracetic acid and the elevation of the temperature to 60 °C. After 2–3 days of stirring at 60 °C the precipitate was filtered off and the resulting black microcrystalline material, presumably product **2e**, was washed with hot chloroform several times. The NMR data of the black solids, which were partially soluble in CDCl_3 and obtained from different trial reactions, were inconsistent and hard to unambiguously interpret. Elemental analysis data, obtained for both the sample filtered off directly from the reaction mixture and for the sample washed three times with chloroform, showed a general consistency with the composition of

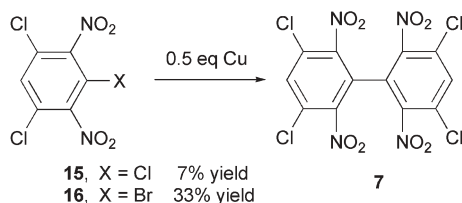


Scheme 3

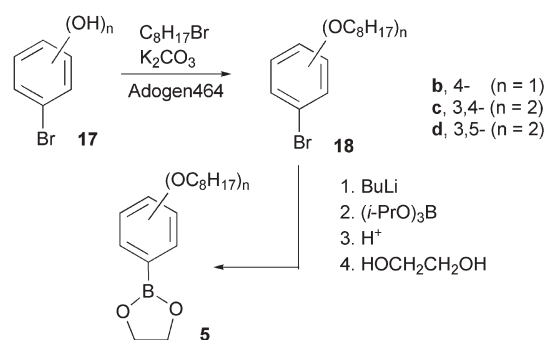
the tetrabromide **2e**. Both analyses showed that the content of carbon was higher by about 1.3%–1.8% relative to that expected for the pure compound. Also, the filtrate obtained after the separation of the black solid (presumably **2e**), poured into water gave a brown solid, which was difficult to purify and analyze. The use of this brown material for Suzuki coupling did not give the expected tetraarylated product, as confirmed by TLC. The black microcrystalline material gave less than 3% of the expected 1,3,6,8-tetraaryl-4,5,9,10-tetraazapyrene in Suzuki reaction with boronic ester **5**.

The preparation of 1,3,6,8-tetrabromophenanthrene (**3e**) is described elsewhere,²⁴ and the synthesis of **4e** followed literature procedure.²⁵

The preparation of tetrachloride **7** was attempted by stoichiometric Ullmann coupling reaction²⁴ of commercially available 1,3,5-trichloro-2,6-dinitrobenzene (**15**) with half an equivalent of freshly prepared copper in 5-*tert*-butyl-*m*-xylene (Scheme 4). However, low regioselectivity and undesired side reactions significantly lowered the yield of pure **7** and complicated its purification. Therefore, 1-bromo-3,5-dichloro-2,6-dinitrobenzene²⁶ (**16**) in dry xylenes was used instead for Ullmann coupling giving **7** in 33% yield (or 72% based on recovered starting **16**).



Scheme 4

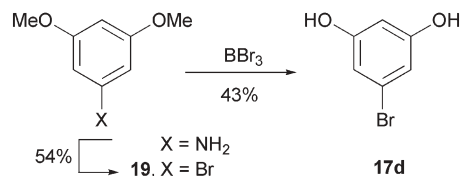


Scheme 5

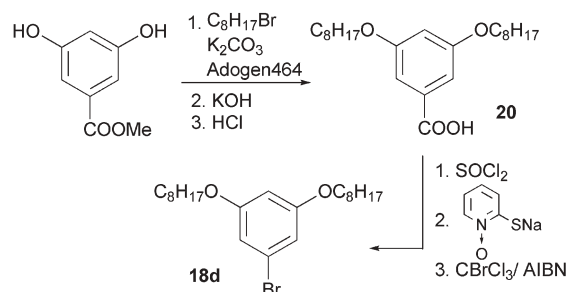
Boronic esters. Boronic esters **5** were prepared according to a general method,²⁷ in which the appropriate octyloxy bromobenzenes **18**, prepared by O-alkylation of bromophenols **17**, were treated with *n*-butyllithium followed by triisopropyl borate (Scheme 5). Esterification of the resulting boronic acids²⁸ with ethylene glycol afforded boronic esters **5**, which were easy to purify by distillation and/or recrystallization.

5-Bromopyrocatechol (**17c**) was prepared from 5-bromosalicylaldehyde using the literature procedure.²⁹

3,5-Dioctyloxybromobenzene (**18d**) was prepared in two ways. In the first method, 3,5-dimethoxyaniline was diazotized and converted to bromo-3,5-dimethoxybenzene (**19**).³⁰ The methyl groups were removed with BBr₃³¹ (Scheme 6) and the resulting 5-bromoresorcinol (**17d**) was alkylated with 1-bromooctane to form **18d** in an overall yield of 22%. Given the relatively high cost for the aniline, we explored another route to **18d** starting from 3,5-dihydroxybenzoic acid (Scheme 7). According to a literature procedure, 3,5-dihydroxybenzoic acid was converted to its methyl ester,³¹ which was O-alkylated with 1-bromooctane and subsequently hydrolyzed.³² The resulting 3,5-dioctyloxybenzoic acid (**20**) was transformed to **18d** using a Barton reaction procedure for an analogous compound.³³ The intermediate acid chloride was obtained

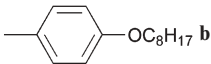
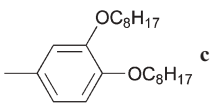
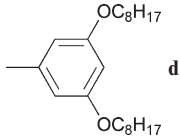
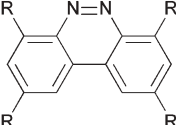
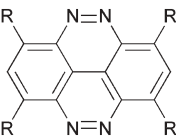
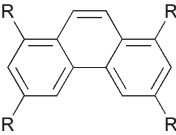
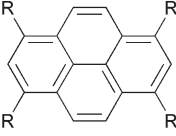


Scheme 6



Scheme 7

Table 1 Transition temperatures and enthalpies for derivatives **1–4**^a

			
	Cr 133 59 I	Cr ₁ 19 5 Cr ₂ 92 12 Col _h 168 20 I [Col _h 32] ^b I	
	Cr 161 39 I	Cr ₁ 46 3 Cr ₂ 95 69 Col _h 199 11 I Cr 45 92 I	
	Cr 152 73 I	Cr 101 44 I	^c
	Cr ₁ 67 43 Cr ₂ 95 — Cr ₃ 116 50 I ^d	Cr 73 55 Col _h 87 24 I	Cr 81 25 [Col _h 25] ^b I

^a Transition temperatures (°C) and enthalpies (in italics, kJ mol⁻¹) were determined by DSC (10 °C min⁻¹; 5 °C min⁻¹ for **2**) in the heating mode: Cr = crystalline; Col_h = columnar hexagonal; I = isotropic. ^b Virtual isotropic transition. ^c Not investigated. ^d Melting at 89 °C followed by crystallization at 95 °C. See text for details.

from acid **20** as a dark oil, which partially decomposed upon attempted vacuum distillation. Therefore, the acid chloride was used as a crude product, giving the bromide **18d** in a moderate overall yield of 41% based on **20**.

Liquid crystalline properties

Tetraaryl derivatives **1–4** (except for **3d**) and biphenyls **6** were investigated by polarized optical microscopy (POM) and differential scanning calorimetry (DSC) for mesogenic behavior. Five of them were subsequently studied by variable temperature powder X-ray diffraction (XRD). Results of DSC analysis for **1–4** are collected in Table 1 and XRD data are shown in Table 2.

Polarized optical microscopy (POM). Optical investigations showed that only three compounds with 3,4-dioctyloxyphenyl substituents, **1c**, **2c**, and **4c**, exhibit liquid crystalline behavior. The mesophase of **2c** and **4c** supercooled forming a glass at room temperature. Neither phenanthrene derivative **3b** nor **3c** exist as liquid crystalline material. Mesophases obtained on cooling of the three mesogenic compounds exhibited fan- or flower-shaped textures, which are characteristic for columnar phases³⁴ (Fig. 1). The texture of benzo[*c*]cinnoline derivative **1c** also displayed domains typical for homeotropically oriented

regions of a uniaxial phase (Fig. 1a). Upon cooling, **1c** formed a rigid phase, which optically was not different from the preceding mesophase. This observation was confirmed by DSC, and on the basis of XRD analysis (*vide infra*) it was tentatively assigned as a columnar crystal (Cr_{col}). The intense dark red color of tetraazapyrene derivative **2c** did not allow for a detailed optical analysis of its texture.

Other compounds in the series **1–4**, except for **1d**, showed only melting to an isotropic phase upon heating, and crystallization upon cooling, often exhibiting significant supercooling of the isotropic phase. Benzo[*c*]cinnoline derivative **1d** exists as an isotropic liquid. Analysis of biphenyls **6b–6d** showed no liquid crystalline behavior even in samples supercooled by up to 10 °C.

Differential scanning calorimetry (DSC). DSC analysis confirmed optical observations that only **1c**, **2c**, and **4c** exhibit liquid crystalline properties (Table 1). Benzo[*c*]cinnoline **1c** showed three transitions. On cooling, the 168 °C transition showed practically no hysteresis, while the two others exhibited a modest supercooling by 6 °C for the 92 °C transition, and 10 °C for the 19 °C transition (Fig. 2). This is consistent with the appearance of progressively more viscous and organized phases. The enthalpy of the clearing transition

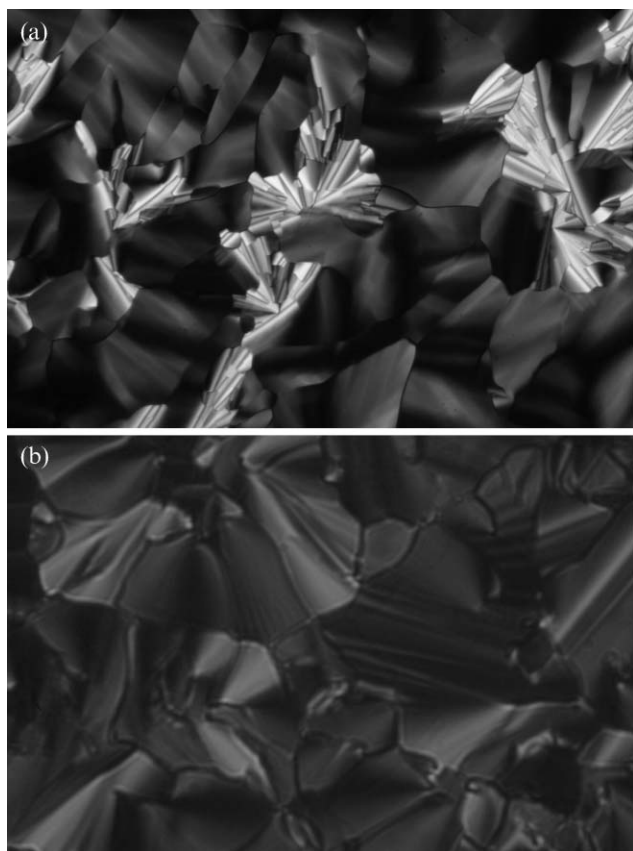


Fig. 1 Optical textures of (a) **1c** at 155 °C and (b) **4c** at 75 °C. Both textures were obtained upon cooling. Magnification $\times 300$.

at 168 °C is 20 kJ mol⁻¹, which is consistent with that for other discotic materials.³⁵

The first heating DSC curve of tetraazapyrene **2c** also showed three transitions, two of which were not observed in the cooling cycle. Consequently, the mesophase was supercooled to ambient temperature, presumably forming a glass. The subsequent heating showed a broad annealing peak and partial crystallization at about 85 °C followed by melting at 99 °C.

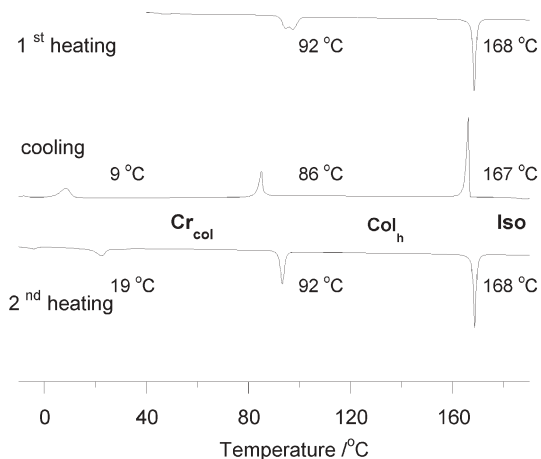


Fig. 2 DSC traces of benzo[c]cinnoline **1c**. The heating rate was 10 °C min⁻¹.

The first DSC heating curve of pyrene **4c** showed a broad transition at about 60 °C followed by two well-defined broad transitions at 73 °C and at 87 °C. The cooling trace displayed only one transition at 77 °C. This shows a bigger hysteresis of the isotropic–discotic transition as compared with the results for **1c** and **2c**. No crystallization peak was observed at a scanning rate of 10 °C min⁻¹, and the hexagonal phase most likely formed a glass phase at room temperature. This is consistent with microscopic observations (*vide supra*). On the second heating curve obtained immediately after the cooling experiment, only a transition at 87 °C with an enthalpy of 18 kJ mol⁻¹ was detected.

DSC thermograms of the remaining compounds generally showed only transitions corresponding to melting and crystallization processes, often with significant supercooling. The only exceptions are benzo[c]cinnoline **1d** and pyrene **4b**. The former exists as an isotropic liquid and DSC analysis did not detect any transition upon cooling to -120 °C. The thermal behavior of pyrene derivative **4b** is exceptional in the series, since the compound exhibits rich crystalline polymorphism with a peculiar melting–crystallization transition at 89 °C and 95 °C (Fig. 3). Solid and liquid coexist in this range of temperatures and are clearly observed under the microscope. A similar phenomenon was observed previously for a calamitic liquid crystal.³⁶ Upon cooling, the isotropic liquid of **4b** was supercooled by about 45 °C and the material partially crystallized over a range of 30 °C. Subsequent heating of the sample revealed a continued crystallization in the range of 35 °C–60 °C. The Cr–Cr transition at 67 °C observed for the virgin sample was absent but the melting–crystallization and the subsequent melting transitions were fully reproduced. Similar behavior of **4b** was recently reported in the literature.³⁷ The published DSC data indicate that the sample was largely glassified during the crystallization process (crystallization peak at 51 °C). Also the peaks with negative enthalpies at 89.5 °C and 112.5 °C in the reported³⁷ DSC trace are most likely due to evaporation of solvents (ethanol and toluene) trapped in the solid during crystallization. This underscores the necessity of verifying compound purity with combustion analysis.

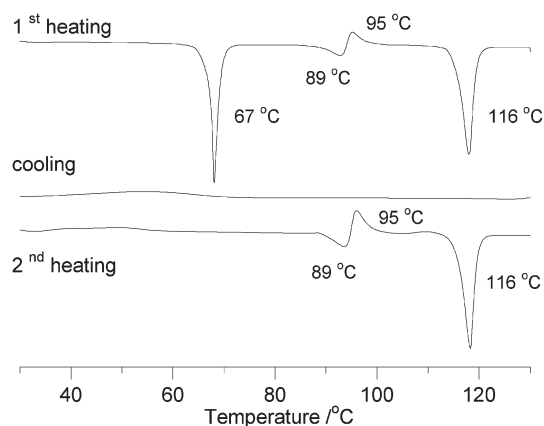


Fig. 3 DSC traces of pyrene derivative **4b**. The heating rate was 10 °C min⁻¹.

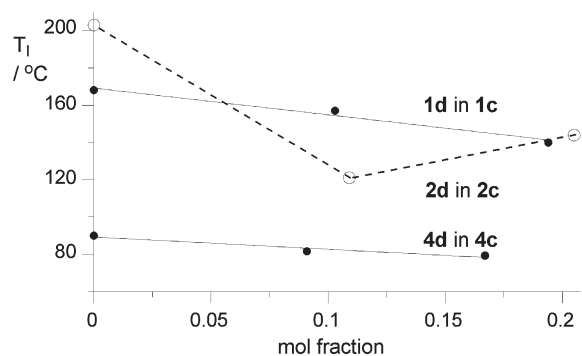


Fig. 4 Clearing temperature T_1 taken as the peak of the transition vs. mol fraction of **1d** in **1c** and **4d** in **4c**. The extrapolated virtual clearing temperatures: 32 ± 11 °C for **1d** ($r^2 = 0.97$) and 26 ± 5 °C for **4d** ($r^2 = 0.95$).

Binary mixtures. Virtual isotropic transitions of the non-mesogenic 3,5-dioctyloxy derivatives **d** were estimated by analysis of binary mixtures with their mesogenic 3,4-dioctyloxy analogs **c** using POM and DSC. Both types of analyses demonstrated broad clearing transitions for solutions containing about 10 mol% and 20 mol% of **d** in **c**. A plot of the transition peak (DSC) vs. concentration for each pair of analogs is shown in Fig. 4.

Both benzo[*c*]cinnoline **1d** and pyrene **4d** decrease clearing temperatures of their 3,4-dioctyloxy derivatives with increasing concentration. For the tetraazapyrene, **2**, the data appear to not follow the sequence observed for **1** and **4**. Linear extrapolation of the data by setting the intercept for each function at the value for the pure host gave virtual transition temperatures for the non-mesogenic derivatives: 32 °C for **1d** and 26 °C for **4d**. The same analysis for **2d** using only the zero and high concentration data points gave the virtual clearing temperature of -77 °C.

Powder X-ray diffraction (XRD). Five compounds in series **1–3** were investigated by powder X-ray diffraction to determine their phase structure. Data were collected at sample-detector distances of 54 and 124 cm at several temperatures chosen typically in the middle of the phase range determined by DSC. XRD results for the mesogenic derivatives **1c** and **2c** are collected in Table 2 and compared to those reported elsewhere for **4c**.³⁸

In a typical experiment, freshly prepared powder samples were analyzed at 25 °C. The non-mesogenic compounds **1b**, **3b**, and **3c** were then analyzed at 80 °C, and subsequently in the isotropic phase. The mesogenic benzo[*c*]cinnoline derivative **1c** was analyzed in the isotropic phase, cooled to a mesophase, and finally measured again at room temperature. The tetraazapyrene **2c** was analyzed only in the heating mode.

Analysis of freshly prepared samples at 25 °C showed a single sharp reflection in the small angle region and a variety of features at higher angles in all five compounds. Indexing of the first few diffraction peaks allow for the tentative determination of two out of the three unit cell dimensions for **1b** ($a = 31.8$ Å and $b = 29.2$ Å) and **3b** ($a = 21.5$ Å and $b = 26.5$ Å). The diffractograms for **1c**, **2c**, and **3c** had only poorly resolved features in the wide angle region, which became sharper upon

Table 2 X-Ray diffraction data

Sample	Temp/°C	phase	<i>hkl</i>	<i>d</i> /Å	Cell const./Å	
1c	130	Col _h	100	25.3	$a = 29.2^a$	
			110	14.6 ^b		
			200	12.7 ^b		
			halo	4.55 ^b		
			001	3.5 ^b		
2c	141	Col _h	100	25.2	$a = 29.1^a$	
			210	9.5		
			halo	4.4		
			001	<3.7		
			100	25.6		$a = 28.9^a$
			110	14.1		
200	12.5					
210	9.5					
4c^c	80	Col _h	300	8.2	$a = 28.9^a$	
			220	6.9		
			400	6.2		
			500	4.9		
			halo	4.55		
			001	3.9		

^a Indexed to a hexagonal lattice: $a = d_{100} \times 2/\sqrt{3}$. ^b The wide-angle data for **1c** were collected using the Scintag system (see ESI), while the other data were collected with the HiStar area detector. ^c Ref. 38.

annealing at 80 °C. This indicates that, in contrast to the mono-octyloxy derivatives, compounds **1c–3c** form poorly ordered crystalline phases, presumably due to lower symmetry of the molecules and a stronger tendency to disorder.

In the isotropic phase the benzo[*c*]cinnoline and phenanthrene derivatives exhibited a typical diffuse feature at about 22 Å, which corresponds to short-range intermolecular correlations. In addition, phenanthrene derivatives **3b** (161 °C) and **3c** (137 °C) showed a broad feature with a maximum at about 4.5 Å, which for benzo[*c*]cinnolines **1b** (140 °C) and **1c** (179 °C) presumably appears outside the measurement window ($2\theta > 23^\circ$).

Analysis of benzo[*c*]cinnoline **1c** and tetraazapyrene **2c** in temperature regions identified to be liquid crystalline showed diffraction patterns that can be ascribed to a two-dimensional hexagonal columnar lattice.³⁹ Both compounds display a sharp high intensity peak at *d* of about 25 Å indexed as the (100) peak (Fig. 5) which corresponds to a cell parameter *a* of about 29 Å (Table 2). The benzo[*c*]cinnoline **1c** also displays two much weaker higher order reflections in the expected spacing

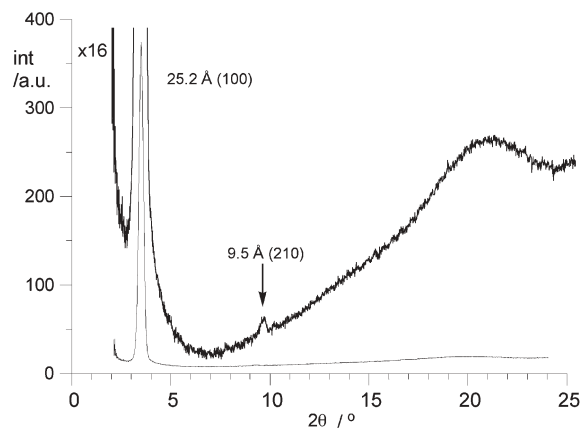


Fig. 5 X-Ray diffraction pattern for **2c** at 141 °C.

ratio of $d_{100}/\sqrt{3}$ and $d_{100}/2$, which are indexed as the (110) and (200) peaks.⁴⁰ These reflections are too weak to observe in the diffractogram of **2c**, which shows only a weak (210) peak at $d = 9.5 \text{ \AA}$ (Fig. 5).

The wide-angle data for **1c** and **2c** show a diffuse peak at 4.5 \AA which arises from correlations between molten alkyl chains. The diffractogram⁴⁰ of **1c** also shows a sharper reflection at 3.5 \AA which corresponds to the distance between cores. Unfortunately, the maximum of this peak for **2c** lies outside of the measurement window ($<3.7 \text{ \AA}$). The presence of this reflection as well as its sharpness indicates the degree of intra-columnar correlations of the hexagonal columnar phase.³⁹

Upon cooling to ambient temperature, the wide-angle diffraction pattern shows that the hexagonal mesophase of tetraazapyrene **2c** crystallized. In contrast, the diffraction pattern of benzo[*c*]cinnoline **1c** changed very little and no additional reflections appeared in the WAXS diffractogram. The only noticeable change is a split of the 100 peak. This suggests the formation of a glass phase with a rectangular or oblique structure, tentatively assigned as Col_r.

Molecular modeling

To gain a better understanding of the observed phase behavior of and XRD results for compounds in series **1–4**, we performed detailed conformational analysis of relevant molecular fragments and also derivatives **2** as representative for the series.

Inspection of the general molecular model **I** (*vide supra*) shows that the overall geometry of compounds **1–4** depends mainly on three factors: *i*) orientation of the phenyl substituent relative to the central core, *ii*) orientation of the alkoxy substituents relative to each other and to the phenyl ring, and *iii*) conformational properties of the alkyl chains. In addition, the energy required to place the phenyl ring co-planar with the central core (planarization energy) indicates the compressibility of the stacks and minimization of the core–core mean distance in the columnar phase.

The phenyl–central core conformational properties and the height of the rotational barrier were assessed at the DFT and MP2 levels of theory using compounds **21a–21c** as models representing the key fragment of the molecule (Fig. 6).

Results collected in Table 3 show that the smallest deviation from co-planarity and smallest planarization energy are

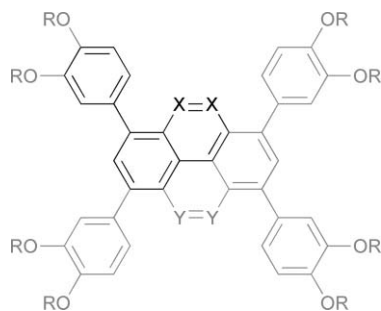
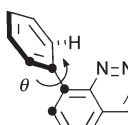
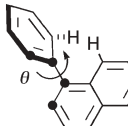
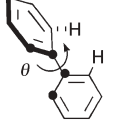


Fig. 6 Phenyl derivatives **21** (outlined) as fragments of **1c** (**21a**: X = N, Y = H; **21c**: X = H, Y = N), **2c** (**21a**: X = Y = N), **3c** (**21b**: X = CH, Y = H; **21c**: X = H, Y = CH), and **4c** (**21b**: X = Y = CH).

Table 3 Rotational transition state energies for phenyl derivatives **21**^a

Compound	ΔE^\ddagger	ΔH^\ddagger	ΔG^\ddagger	θ
	DFT MP2	DFT MP2	DFT MP2	DFT MP2
 21a <i>C_s</i> ^b	4.0	3.5	4.9	43
	6.6	6.1	7.4	46.5
 21b <i>C₁</i> ^b	12.6	12.1	13.4	55
	15.2	14.7	16.0	57 (exp. 60–65) ^c
 21c <i>D_{2h}</i> ^b	2.1	1.6	2.9	38
	3.9	3.4	4.8	45 (exp. 45) ^d

^a DFT calculation at the B3LYP/6-31G(d) level of theory and MP2 at the MP2(fc)/6-31G(d) level with DFT thermodynamic corrections. Energies in kcal mol⁻¹ and angles in °. The GS geometry dihedral angle θ is defined by marked atoms in each structure. ^b Symmetry of the TS. ^c Ref. 41. ^d Ref. 42.

observed for biphenyl (**21c**). These values are moderately larger for cinnoline **21a**, but significantly greater for 1-phenylnaphthalene (**21b**). A comparison of the computational results with scant literature data shows that the MP2 method gives more accurate results than the DFT method. Thus, biphenyl was found to have a 45° dihedral angle between the benzene ring planes in the gas phase,⁴² while in the solid state the crystal packing forces largely overcome the hydrogen–hydrogen interactions and biphenyl is nearly planar.⁴³ In 1-phenylnaphthalene (**21b**) this dihedral angle is larger and between 59°–66°, according to other quantum mechanical calculations⁴⁴ and solution phase experiments.^{41,45}

Detailed analysis of the computational results shows that in the equilibrium geometry the non-bonding N \cdots H and H \cdots H distances in the cinnoline and naphthalene derivatives, **21a** and **21b**, are calculated at about 2.6 Å at the MP2 level of theory, while the DFT method predicts these distances shorter by 0.05 Å. The H \cdots H distance calculated for biphenyl by the two methods is shorter (2.45 Å and 2.37 Å) and comparable with the sum of van der Waals radii (2.4 Å). This difference in the H \cdots H separations is consistent with the smaller dihedral angle θ for biphenyl (**21c**, 45°) than for 1-phenylnaphthalene (**21b**, 57°). In the rotational transition state, cinnoline **21a** and biphenyl **21c** adopt planar structures in which the N \cdots H and H \cdots H distances decrease to 2.08 Å and 1.95 Å, respectively, according to the MP2 results. Steric interactions of the hydrogen atoms in the naphthalene derivative **21b** prevent the formation of the planar transition state. Instead, the naphthalene ring is warped ($\theta = 8.5^\circ$ at DFT and $\theta = 11.7^\circ$ at MP2) and the H \cdots H distance is very short (1.62 Å at DFT and 1.68 Å at MP2).

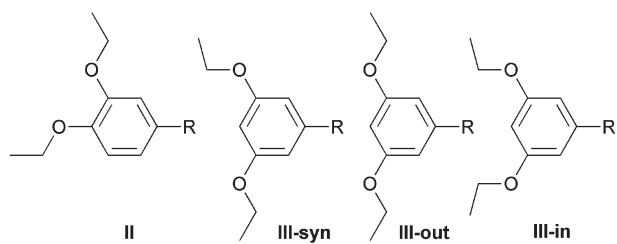


Fig. 7 Arrangement of two alkoxy substituents. Only the first two carbon atoms are shown for simplicity.

Conformational properties of the alkoxy chains were assessed based on literature reports, and their impact on the molecular shape of **1–4** was evaluated using molecular mechanics. A literature search revealed several solid-state structures containing either the 3,4-dialkoxyphenyl (**II**) or 3,5-dialkoxyphenyl (**III**) substituents (Fig. 7). In the former the two vicinal alkoxy groups are coplanar with the benzene ring and the alkyl chains extending in opposite directions (Fig. 7).^{46–48} To improve crystal packing, one^{46,48} or both⁴⁷ alkyl chains adopt a *gauche* conformation so that the two chains can propagate parallel to each other. The two solid state structures of 3,5-dialkoxyphenyl (**III**) reported in the literature^{49,50} indicate that the two substituents are coplanar and propagate in the same direction (a *syn* orientation). The other two symmetric orientations of the alkoxy chains (*out* and *in*) have not been reported.

Orientation of the alkoxy substituents shown in Fig. 7 suggested the starting points for molecular geometry optimizations of tetraazapyrenes **2c** and **2d** as representatives for the series. For simplicity only one dialkoxyphenyl substituent was included, and the structures were optimized using the universal force field (UFF) algorithm. Initially, both alkyl chains were set in all-*trans* conformation coplanar with the phenyl ring and results of geometry optimization for the 3,4-dioctyloxy- and *syn* and *in* 3,5-dioctyloxyphenyl derivatives are shown in Fig. 8. Subsequently a *gauche* conformation was introduced between the C1 and C2 atoms in the octyloxy chain at the 3 position of the 3,4-derivative, and in both chains of the 3,5-derivative. In all calculations, the torsional angle between the phenyl ring and the heterocycle was about 50°,

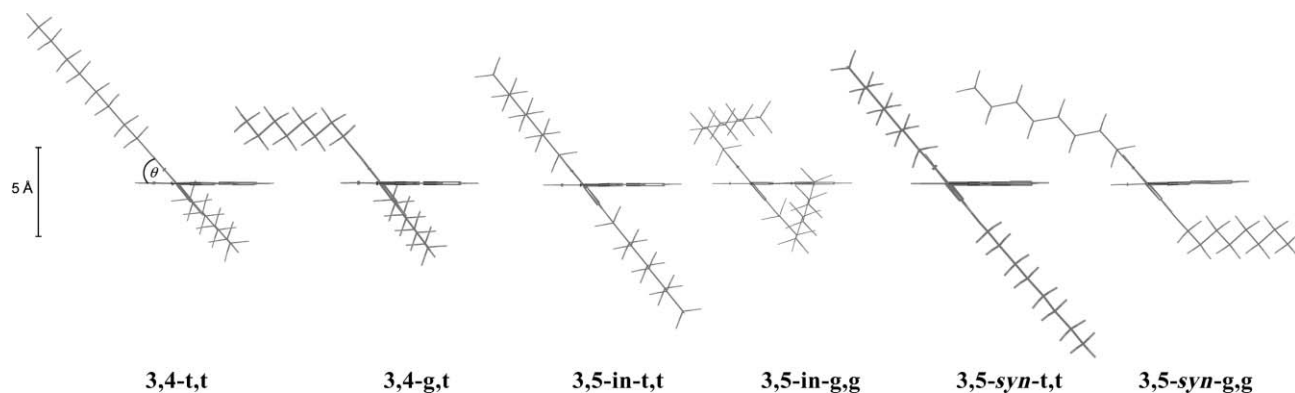


Fig. 8 Selected conformers of model for **2c** and **2d** viewed along the plane containing the central heterocycle. For clarity only one dioctyloxyphenyl substituent is used in the modeling. Geometry was optimized with universal force field for alkyl chains in *trans* and *gauche* conformation imposed for the C1–C2 bond.

which compares well with the calculated 46.5° for phenylcinoline (**21a**, Table 3).

Results in Fig. 8 show that for the all-*trans* conformers, the width of the molecule is smallest for the 3,4-derivative **3,4-t,t** (13.5 Å) and the largest for **3,5-syn-t,t** (17.5 Å) and it scales with $\sin\theta$ where θ is the angle between the phenyl ring and the heterocycle. Introduction of the *gauche* conformation at the C1–C2 bond, at a cost of about 0.9 kcal mol⁻¹ per bond, significantly lowers the molecular extent in the *z* direction. The molecular thickness for **3,4-g,t** and **3,5-g,g** derivatives with two *gauche* conformations is about 9 Å. It can be estimated that for the molecular width of 3.7 Å, consistent with the XRD data, the angle θ should be about 18°, instead of 50° calculated for an isolated molecule.

Projections in Fig. 8 hint at difficulties in accommodation of 3,5-dioctyloxyphenyl substituents in the planarized conformations (small θ). Analysis suggests that a significant number of *gauche* conformations are required for achieving geometry favorable for the formation of a mesophase. In contrast, in the 3,4-dioctyloxy derivatives one *gauche* conformation in the 3-octyloxy chain is sufficient for significant “flattening” of the molecule and the 4-octyloxy chains, that are projected outwards, do not hinder the planarization of the phenyl–heterocycle torsional angle θ . A projection of a geometry-optimized molecule of **2c** with one possible orientation of the 3,4-octyloxyphenyl rings is shown in Fig. 9. It is conceivable that the second molecule will adopt an orientation 90° rotated relative to the first molecule to fill in the gap. Such a possibility was suggested for another derivative of pyrene.³⁷

Electronic structure

To estimate charge accepting abilities of the discotics, energies for the two frontier molecular orbitals (FMOs) of the central core elements **1a–4a** and a pair of triphenylene–hexaazatriphenylene were calculated at the MP2/6-31G(d) level of theory. Results in Fig. 10 show that among the three hydrocarbons, pyrene (**4a**) has the highest lying HOMO (−6.87 eV) and hence it is the best electron donor. Conversely, its tetraaza analog, **2a**, has the lowest LUMO energy (0.30 eV) among the three heterocycles, and it appears to be the best electron acceptor in the series. The substitution of N atoms into pyrene shifts the

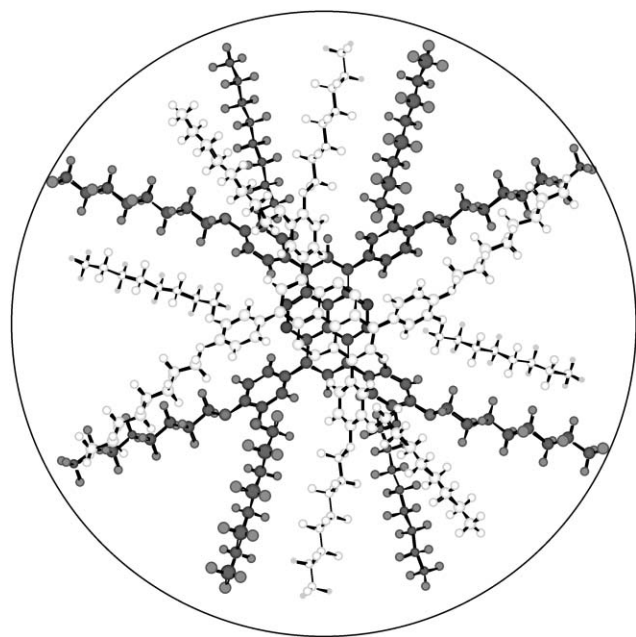


Fig. 9 A view of the most extended conformation of **2c** along the z axis perpendicular to the heterocycle plane. Conformation of each substituent corresponds to **3,4-g,t** in Fig. 8. The geometry of **2c-g,t** was constrained in the C_s symmetry and minimized using the PM3 method. The inscribed circle has a diameter of 36 Å.

FMOs by about 1.5 eV, which is about 50% more than observed in the phenanthrene–benzo[*c*]cinnoline pair. Trends shown in Fig. 10 are consistent with generally observed trends in experimental redox potentials, electron affinities, and ionization potentials (for details see ESI†).

Electronic absorption spectroscopy

UV-Vis absorption spectra for the 4-octyloxyphenyl derivatives **1b–4b** in cyclohexane are shown in Fig. 11. Substitution of the parent compounds **1a–4a** with four 4-octyloxyphenyl

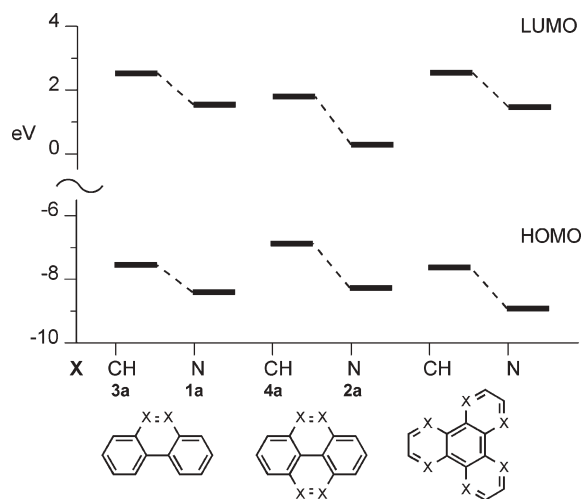


Fig. 10 The HOMO and LUMO energy levels for hydrocarbons and their aza analogs obtained at the MP2/6-31G(d) level. Numerical values are listed in the ESI.

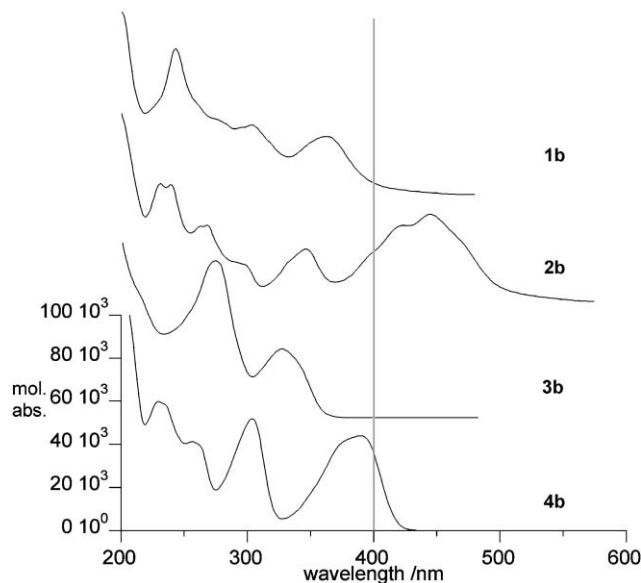


Fig. 11 UV-Vis spectra for 4-octyloxyphenyl derivatives of benzo[*c*]cinnoline **1b**, tetraazapyrene **2b**, phenanthrene **3b**, and pyrene **4b** recorded in cyclohexane. Each spectrum is plotted in $0\text{--}10^5$ molar absorptivity scale and the spectra are stacked for clarity. The vertical line marks the UV-Vis border.

groups results in a red-shift of their absorption bands. Among the four compounds, only the phenanthrene derivative **3b** is a colorless solid. The longest wavelength absorption bands in **1b** and **4b** tail in to the visible region (the gray vertical line in Fig. 11) giving them a yellowish color. Compound **2b** has two intense absorption bands in the visible region which give it the dark red color.

The moderate intensity ($\log \epsilon = 2.4$)⁵¹ L_b band in benzo[*c*]cinnoline **1a** appears to be shifted in **1b** by about 30 nm to 373 nm ($\log \epsilon = 4.46$). Substitution in the parent tetraazapyrene **2a** red-shifts its two longest wavelength absorption bands, at 373 nm ($\log \epsilon = 3.79$, EtOH) and 391 nm ($\log \epsilon = 3.87$, EtOH),⁵² by about 70 nm in **2b**. In the parent phenanthrene **3a** the longest wavelength L_b band ($\log \epsilon = 2.4$)⁵¹ is replaced with an intense band with a maximum at 335 nm ($\log \epsilon = 4.53$) in **3b**. This band is likely to be related to the L_a band of **3a** red-shifted in **3b** by about 40 nm. The lowest energy absorption band for pyrene **4b** has a maximum at 390 nm ($\log \epsilon = 4.64$), which is shifted by 55 nm relative to the allowed 1L_a transition or 35 nm relative to the forbidden 1L_b band in pyrene (**4a**).⁵³

Discussion

Analysis of results in Table 1 demonstrates the significance of conformational, steric, and packing density (space filling) effects on mesophase stability. A comparison of the effectiveness of the substituents **b–d** in phase stabilization shows that only 3,4-dioctyloxyphenyl (**c**) induces mesogenic behavior presumably by striking a balance between the density of the alkyl chains and their preferred orientation. The octyl group of the mono-octyloxyphenyl substituent (**b**) propagates in the plane close to that of the central core but the alkyl chain density (fill fraction) is apparently too low to support a

mesogenic state. Addition of a second chain in the 3-position in **c** provides the necessary density for appearance of a mesophase apparently at the modest expense of one *gauche* conformation (Fig. 8). A similar induction of a columnar mesophase was observed for other pairs of compounds.^{38,54} Moving the octyloxy group from position 4 to 5 in substituent **d** increases steric interference of the alkyl chains and hinders molecular planarization. This leads to a significant broadening of the molecule and to a lower fill fraction. Consequently, the mesophases are dramatically destabilized by 136 °C for **1d** and 64 °C for **4d**, as estimated from binary mixtures. In these derivatives, the contact between the rigid cores is so difficult that compounds have either low melting points (*e.g.* **2d**) or are liquids at ambient temperature (**1d**, see also ref. 38). Also, the experienced difficulties with crystallization and purification of **3d** can be largely ascribed to the significantly hindered core–core contact. The unusually low enthalpy of melting for **4d** is presumably also due to the poor packing and loose core–core contact.

The significance of the high fill fraction for mesogenic compounds is demonstrated by a pair of discogens **1c** and **2c**. At first glance it would appear that the moderate dipole moment of the benzo[*c*]cinnoline ring and more compressible biphenyl-type torsional angles in **1c** would result in higher stability of the mesophase. Experiment shows, however, that incorporation of another azo group into the central heterocycle increases the clearing temperature by over 30 °C in **2c**, in spite of the loss of the net molecular dipole moment and increase of the planarization barrier for two substituents in **2c**. It is plausible that this stabilization of the mesophase is related to the higher fill fraction of the central core in **2c** than in **1c**. This appears to be valid also for the pair **3c** and **4c** for which the difference in the mesophase stability is at least 60 °C.

The third type of structural effect on the mesophase thermodynamic stability is the heteroatom substitution in the central core. In a pair of such discogens, **2c** and **4c**, the observed effect is pronounced. The substitution of the four CH groups in **4c** with nitrogen atoms in **2c** increases the clearing temperature by over 110 °C. This is consistent with the results for the triphenylene–hexaazatriphenylene pair in which the clearing temperature difference is 59 °C.⁵⁴ This significant stabilization may be due to stronger quadrupolar interactions between the cores in the former, and may also result from fewer H···H steric interactions. The latter gives rise to greater compressibility of the Ph–core dihedral angle, and consequently closer contact of the rigid cores within the column. A comparison of the core–core correlation peak in the wide-angle region of the XRD data provides information on the intracolumn packing, and ability of the molecules to adopt the planar conformation. The core–core separation appears to be the largest for pyrene derivative **4c** (3.9 Å), while for benzo[*c*]cinnoline **1c** the mean distance is the smallest in the series (3.5 Å) and typical for discogens.³⁹ (For tetraazapyrene **2c** the 001 peak presumably is below 3.7 Å.) The core–core separation typically shows only a weak temperature dependence so the comparison of the data for pyrene **4c**, taken close to the transition point, and **1c** and **2c** further away from the clearing point should still hold. Even the carbazole analog of **4c** at 120 °C near the clearing point has a core–core spacing of

3.7 Å.³⁸ These large differences in the core–core distance can be related to the planarization energy for each phenyl group. Thus, the largest intermolecular separation is observed for pyrene, which is consistent with the steepest rotational potential for the Ph–pyrene bond with the maximum at about 15 kcal mol^{−1}. In contrast, for tetraazapyrene and benzo[*c*]cinnoline this potential energy curve has a maximum of only about 6 kcal mol^{−1} and the dihedral angle between the phenyl and the core can be compressed more easily.

Modeling results show that dimensions for molecules with the most extended chains (*cf.* Fig. 9) are about 7 Å larger than the intercolumnar distance established by XRD. This suggests that the last few methylene units are “melted” and folded up, which is consistent with the observed diffraction patterns and abnormal intensity of the (110) and (200) peaks for **2c** and **4c**.

The low intensity, or even absence, of (110) and (200) reflections in the X-ray diffraction pattern of **2c** (Fig. 5) was unexpected, although similar situations have been previously observed in molecules with unusual charge distributions.^{55–58} Indeed, for columnar derivatives of [5]helicene⁵⁶ and triphenylene⁵⁷ the intensity of the (110) reflection was almost zero, the (200) was more intense, and the strongest higher-order reflection was the (210). A very similar situation is observed in the diffraction pattern of **2c** in which only the (210) higher-order reflection is clearly visible and the (110) and (200) are at the noise level. In the diffraction pattern of **4c**, a close analog of **2c**, the (110) and (210) peaks are very weak.³⁸

A plausible explanation of this apparent anomaly in the diffraction pattern of **2c** is provided by the predicted X-ray scattering intensity calculated from the square of the Fourier transform of the molecular charge density.⁵⁹ Calculations performed for the most extended conformer of **2c-g,t** (Fig. 9) show intensities of the higher order reflections typical for the columnar phase: the (110) and (200) signals in the high amplitude region and the (210) is in the minimum of the structure factor (Fig. 12). This is observed for **1c** but is inconsistent with the results for **2c**. Folding up of the alkyl chain ends

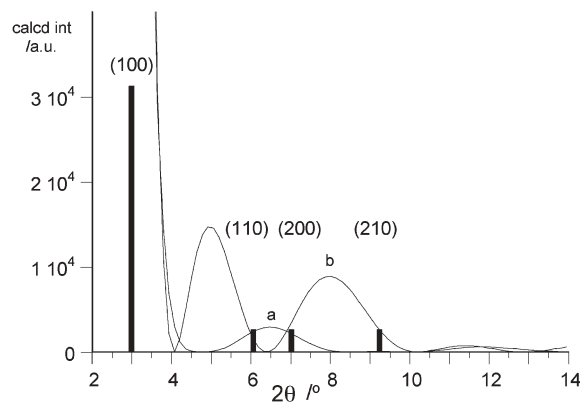


Fig. 12 Relative calculated scattered intensity for **2c-g,t** (a) with most extended alkyl chains (Fig. 9) and conformer **2c-melted** (b) with ends of alkyl chains “melted” and folded back (Fig. 13). The intensity was calculated from the square of the Fourier transform of the cylindrically averaged molecular charge density, including the $1/(\sin\theta \sin 2\theta)$ Lorentz factor. The vertical bars show the positions of expected reflections for the Col_h phase of **2c**.

in **2c-g,t** and decreasing the molecular diameter to 29 Å, consistent with the unit cell parameter a , results in a reduction of the mean charge density radius and a concomitant increase in the angles of characteristic features in the structure factor. This shifts a minimum in the structure factor to the region near the (110) and (200) peaks, and increases the amplitude of the (210) peak. Thus, increasing the density of *gauche* bonds in the alkyl chain has the general effect of reducing the mean radius of the charge density, reducing the intensity of the (110) and (200) peaks and increasing the amplitude of the (210) peak. Given the small number of measured diffraction intensities and the large number of spatial degrees of freedom for the molecule, we did not attempt to refine molecular parameters to fit the data. Nonetheless, the observed trend in the calculated structure factor and molecular shape is consistent with the experimentally observed intensity of higher order reflections and the unit cell parameter a .

Conclusions

A series of compounds **1–4** provided a rare opportunity to demonstrate the significance of the fill fraction in stabilization of discotic phases. Analysis suggested that the fill fraction is affected by the conformational properties of the Ph–core junction and the distribution and density of the alkyl chains. The presence of N atoms lowers planarization barriers, the 3,4 substitution pattern allows for the phenyl rings to planarize without significant alkyl chain–alkyl chain interactions and necessity of a high density of *gauche* conformations. In addition, the higher fill fraction is obtained with a more

condensed central core. It is also expected that the permanent dipole moment in benzo[*c*]cinnoline derivatives **1** and high quadrupolar moment in tetraazapyrene **2** further stabilize the liquid crystalline phases, but these effects appear to be secondary to geometrical and steric factors. Consequently, tetraazapyrene derivative **2c** has the most stable and phenanthrene derivative **3c** has the least stable mesophases in the series.

Calculations demonstrated that high electron deficiency is achieved by using the azo group as part of the heterocycle skeleton. Thus, tetraazapyrene discogen **2c**, containing two such groups, has a low-lying LUMO and appears to be suitable for electron transport. However, the azo moiety shifts the electronic absorption to the visible range which may be undesirable for some applications.

Analysis of XRD patterns demonstrated that the intensity of the higher order reflections may differ significantly from typical and expected values, and can be related to the molecular structure and packing in the columnar phase.

Computational details

Quantum-mechanical calculations were carried out with the B3LYP/6-31G(d) and MP2(fc)/6-31G(d) methods using the Linda-Gaussian 98 package⁶⁰ on a Beowulf cluster of 14 processors. Geometry optimizations were undertaken using appropriate symmetry constraints and default convergence limits. Vibrational frequencies were calculated with the DFT method and were used to characterize the nature of the stationary points and to obtain thermodynamic parameters. Zero-point energy (ZPE) corrections were scaled by 0.9806.⁶¹ The DFT-optimized ground and transition state structures were used as starting points for MP2 geometry optimizations. Geometry optimizations were carried out using the Universal Force Field algorithm supplied with the Cerius2 suite of programs.

Experimental

The purity of samples was determined by HPLC analysis using a normal phase column and a gradient hexane–CH₂Cl₂ mixture. Samples of liquid crystalline materials were prepared using a pair of virgin microscopic cover glass plates and observed in polarized light using a PZO Biolar PI microscope consisting of polarizer, analyzer, and the HS1 Instec hot stage. Samples were heated and cooled at rates of 5 °C min⁻¹ or 10 °C min⁻¹. Thermal data were obtained on a TA Instrument DSC-2920 calibrated with an indium standard. Preliminary XRD measurements on **1c** employed a Scintag X1 Advanced Diffraction System. Further measurement, carried out at the University of Pennsylvania, Philadelphia, employed a Bruker-Nonius FR591 fine-focus generator with a Cu target ($\lambda = 1.542$ Å) mirror-monochromator optics, and a Bruker HiStar wire detector. 2D diffraction patterns were subsequently reduced to plots of scattered intensity *versus* 2θ , where θ is related to d -spacing by $d = \lambda/2\sin(\theta)$. In comparison with the Scintag measurements, data collected with the HiStar detector had higher angular resolution and lower spectral contamination but did not extend to as high an angular range.

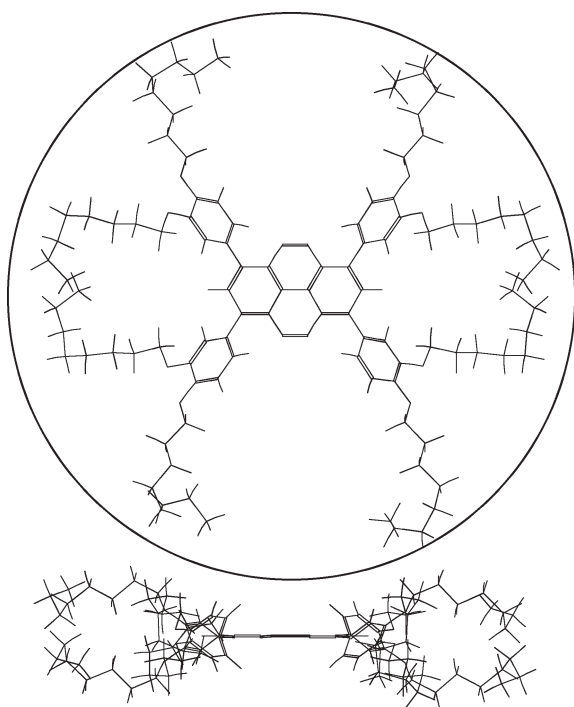


Fig. 13 Conformer **2c-melted** with the “melted” alkyl chain ends of **2c-g,t** viewed along the z axis perpendicular to the heterocycle plane (top) and along the heterocycle plane (bottom). The radius of the inscribed circle is 29 Å.

Acknowledgements

This project was supported by the NSF grants (CHE-9528029 and CHE-0096827). We thank Mr. Xuan Sun and Mr. Andy Wenger for their technical assistance. Crystallographic work at the University of Pennsylvania was supported by the MRSEC program of the National Science Foundation (Grant # DMR05-20020).

References

- 1 In part described in: M. J. Sienkowska, Dissertation, Vanderbilt University, 2004; J. M. Farrar, Dissertation, Vanderbilt University, 2001.
- 2 S. Chandrasekhar, in *Handbook of Liquid Crystals*, ed. D. Demus, J. Goodby, G. W. Gray, H.-W. Spiess and V. Vill, Wiley-VCH, New York, 1998, vol. 2B, pp. 749–780.
- 3 S. Chandrasekhar and S. K. Prasad, *Contemp. Phys.*, 1999, **40**, 237–245.
- 4 For a recent overview see: M. O'Neill and S. M. Kelly, *Adv. Mater.*, 2003, **15**, 1135–1146. See also ref. 9.
- 5 G. Lüssem and J. H. Wendorff, *Polym. Adv. Technol.*, 1998, **9**, 443–460.
- 6 I. H. Stapff, V. Stümpflen, J. H. Wendorff, D. B. Spohn and D. Möbius, *Liq. Cryst.*, 1997, **23**, 613–617.
- 7 I. Seguy, P. Jolinat, P. Destruel, J. Farenc, R. Mamy, H. Bock, J. Ip and T. P. Nguyen, *J. Appl. Phys.*, 2001, **89**, 5442–5448.
- 8 L. Schmidt-Mende, A. Fechtenkötter, K. Müllen, E. Moons, R. H. Friend and J. D. MacKenzie, *Science*, 2001, **293**, 1119–1122.
- 9 N. Boden and B. Movaghar, in *Handbook of Liquid Crystals*, ed. D. Demus, J. Goodby, G. W. Gray, H.-W. Spiess and V. Vill, Wiley-VCH, New York, 1998, vol. 2B, pp. 781–798.
- 10 S. Kumar, E. J. Wachtel and E. Keinan, *J. Org. Chem.*, 1993, **58**, 3821–3827.
- 11 N. Boden, R. C. Borner, R. J. Bushby and J. Clements, *J. Am. Chem. Soc.*, 1994, **116**, 10807–10808.
- 12 T. Ishi-i, K. Murakami, Y. Imai and S. Mataka, *Org. Lett.*, 2005, **7**, 3175–3178; T.-H. Chang, B.-R. Wu, M. Y. Chiang, S.-C. Liao, C. W. Ong, H.-F. Hsu and S.-Y. Lin, *Org. Lett.*, 2005, **7**, 4075–4078.
- 13 K. Pieterse, P. A. van Hal, R. Kleppinger, J. A. J. M. Vekemans, R. A. J. Janssen and E. W. Meijer, *Chem. Mater.*, 2001, **13**, 2675–2679.
- 14 R. I. Gearba, M. Lehmann, J. Levin, D. A. Ivanov, M. H. J. Koch, J. Barberá, M. G. Debije, J. Piris and Y. H. Geerts, *Adv. Mater.*, 2003, **15**, 1614–1618.
- 15 G. Kestenont, V. de Halleux, M. Lehmann, D. A. Ivanov, M. Watson and Y. H. Geerts, *Chem. Commun.*, 2001, 2074–2075.
- 16 C. W. Ong, S.-C. Liao, T. H. Chang and H.-F. Hsu, *J. Org. Chem.*, 2004, **69**, 3181–3185.
- 17 M. Lehmann, G. Kestemont, R. G. Aspe, C. Buess-Herman, M. H. J. Koch, M. G. Debije, J. Piris, M. P. de Haas, J. M. Warman, M. D. Watson, V. Lemaure, J. Cornil, Y. H. Geerts, R. Gearba and D. A. Ivanov, *Chem.-Eur. J.*, 2005, **11**, 3349–3362.
- 18 P. Kaszynski, *Molecules*, 2004, **9**, 716–724.
- 19 P. Kaszynski, in *Magnetic Properties of Organic Materials*, ed. P. M. Lahti, Marcel Dekker, Inc., New York, 1999, pp. 305–324.
- 20 N. Miyaura, T. Yanagi and A. Suzuki, *Synth. Commun.*, 1981, **11**, 513–519.
- 21 H. Stetter and M. Schwarz, *Chem. Ber.*, 1957, **90**, 1349–1351.
- 22 J. F. Corbett and P. F. Holt, *J. Chem. Soc.*, 1961, 3695–3699.
- 23 A. E. Blood and C. R. Noller, *J. Org. Chem.*, 1957, **22**, 711–712.
- 24 J. M. Farrar, M. Sienkowska and P. Kaszynski, *Synth. Commun.*, 2000, **30**, 4039–4045.
- 25 K. Ogino, S. Iwashima, H. Inokuchi and Y. Harada, *Bull. Chem. Soc. Jpn.*, 1965, **38**, 473–477.
- 26 J. T. Manka, F. Guo, J. Huang, H. Yin, J. M. Farrar, M. Sienkowska, V. Benin and P. Kaszynski, *J. Org. Chem.*, 2003, **68**, 9574–9588.
- 27 G. W. Gray, M. Hird, D. Lacey and K. J. Toyne, *J. Chem. Soc., Perkin Trans. 2*, 1989, 2041–2053.
- 28 4-Octyloxyphenylboronic acid and 3,4-dioctyloxyphenylboronic acid are known: T. Yatabe, M. A. Harbison, J. D. Brand, M. Wagner, K. Müllen, P. Samori and J. P. Rabe, *J. Mater. Chem.*, 2000, **10**, 1519–1525; S. J. Lock, J. W. Goodby, M. Hird and K. J. Toyne, *J. Mater. Chem.*, 1995, **5**, 2175–2182; M. C. Artal, K. J. Toyne, J. W. Goodby, J. Barberá and D. J. Photinos, *J. Mater. Chem.*, 2001, **11**, 2801–2807.
- 29 H. D. Dakin, *Am. Chem. J.*, 1909, **42**, 477–487; T. V. Hansen and L. Skattebøl, *Tetrahedron Lett.*, 2005, **46**, 3357–3358.
- 30 M. R. Detty and B. J. Murray, *J. Am. Chem. Soc.*, 1983, **105**, 883–890.
- 31 J. H. Birkinshaw and A. Bracken, *J. Chem. Soc.*, 1942, 368–370.
- 32 G. Pickaert and R. Ziessel, *Synthesis*, 2004, 2716–2726.
- 33 G. C. Dol, P. C. J. Kamer and P. W. N. M. van Leeuwen, *Eur. J. Org. Chem.*, 1998, 359–364.
- 34 I. Dierking, *Textures of Liquid Crystals*, Wiley-VCH, Weinheim, 2003.
- 35 V. Vill, LiqCryst 4.6, LCI GmbH, Hamburg, 2004 and references therein.
- 36 P. Kaszynski, S. Pakhomov, K. F. Tesh and V. G. Young, Jr., *Inorg. Chem.*, 2001, **40**, 6622–6631.
- 37 V. de Halleux, J.-P. Calbert, P. Brocorens, J. Cornil, J.-P. Declercq, J.-L. Brédas and Y. Geerts, *Adv. Funct. Mater.*, 2004, **14**, 649–659.
- 38 M. J. Sienkowska, H. Monobe, P. Kaszynski and Y. Shimizu, *J. Mater. Chem.*, 2007, DOI: 10.1039/b612253a.
- 39 S. K. Prasad, D. S. S. Rao, S. Chandrasekhar and S. Kumar, *Mol. Cryst. Liq. Cryst.*, 2003, **396**, 121–139.
- 40 The wide-angle data for **1c** were collected using the Scintag system (see ESI†).
- 41 C. L. Cheng, D. S. N. Murthy and G. L. D. Ritchie, *J. Chem. Soc., Faraday Trans. 2*, 1972, **68**, 1679–1690.
- 42 A. Almenningen, O. Bastiansen, L. Fernholt, B. N. Cyvin, S. J. Cyvin and S. Samdal, *J. Mol. Struct.*, 1985, **128**, 59–76.
- 43 G.-P. Charbonneau and Y. Delugeard, *Acta Crystallogr., Sect. B*, 1977, **33**, 1586–1588.
- 44 J. Cioslowski, P. Piskorz, G. Liu and D. Moncrieff, *J. Phys. Chem.*, 1996, **100**, 19333–19335.
- 45 E. D. Bergmann, M. Rabinovitz, M. J. Aroney, R. J. W. Le Fevré, L. Radom and G. L. D. Ritchie, *J. Chem. Soc. B*, 1968, 1551–1554.
- 46 H. Allouchi, J.-P. Bideau and M. Cotrait, *Acta Crystallogr., Sect. C*, 1992, **48**, 1037–1041.
- 47 H. Allouchi, M. Cotrait, D. Guillon, B. Heinrich and H. T. Nguyen, *Chem. Mater.*, 1995, **7**, 2252–2258.
- 48 S. H. Eichhorn, A. J. Paraskos, K. Kishikawa and T. M. Swager, *J. Am. Chem. Soc.*, 2002, **124**, 12742–12751.
- 49 G. Bocelli and M.-F. Grenier-Loustalot, *Acta Crystallogr., Sect. C*, 1987, **43**, 1221–1223.
- 50 P. B. Rheiner and D. Seebach, *Chem.-Eur. J.*, 1999, **5**, 3221–3236.
- 51 D. N. de Vries Reilingh, R. P. H. Rettschnick and G. J. Hoytink, *J. Chem. Phys.*, 1971, **54**, 2722–2727.
- 52 P. F. Holt and R. Oakland, *J. Chem. Soc.*, 1964, 6090–6094.
- 53 A. C. Benniston, A. Harriman, D. J. Lawrie and S. A. Rostron, *Eur. J. Org. Chem.*, 2004, 2272–2276.
- 54 N. Boden, R. J. Bushby, G. Headdock, O. R. Lozman and A. Wood, *Liq. Cryst.*, 2001, **28**, 139–144.
- 55 S. H. J. Idziak, N. C. Maliszewskyj, G. B. M. Vaughan, P. A. Heiney, C. Mertesdorf, H. Ringsdorf, J. P. McCauley and A. B. Smith, III, *J. Chem. Soc., Chem. Commun.*, 1992, 98–99; J. Malthete, A.-M. Levelut and J.-M. Lehn, *J. Chem. Soc., Chem. Commun.*, 1992, 1434–1436.
- 56 C. Nuckolls and T. J. Katz, *J. Am. Chem. Soc.*, 1998, **120**, 9541–9544.
- 57 M. T. Allen, S. Diele, K. D. M. Harris, T. Hegmann, B. M. Kariuki, D. Lose, J. A. Preece and C. Tschierske, *J. Mater. Chem.*, 2001, **11**, 302–311.
- 58 S. Kumar, J. J. Naidu and D. S. S. Rao, *J. Mater. Chem.*, 2002, **12**, 1335–1341.
- 59 J. Als-Nielsen and D. McMorrow, *Elements of Modern X-ray Physics*, Wiley, New York, 2001.
- 60 M. J. Frisch, G. W. Trucks, H. B. Schlegel, G. E. Scuseria, M. A. Robb, J. R. Cheeseman, V. G. Zakrzewski, J. A. Montgomery, Jr., R. E. Stratmann, J. C. Burant, S. Dapprich, J. M. Millam, A. D. Daniels, K. N. Kudin, M. C. Strain, O. Farkas, J. Tomasi, V. Barone, M. Cossi, R. Cammi, B. Mennucci, C. Pomelli, C. Adamo, S. Clifford, J. Ochterski, G. A. Petersson, P. Y. Ayala, Q. Cui, K. Morokuma, D. K. Malick, A. D. Rabuck,

K. Raghavachari, J. B. Foresman, J. Cioslowski, J. V. Ortiz, A. G. Baboul, B. B. Stefanov, G. Liu, A. Liashenko, P. Piskorz, I. Komaromi, R. Gomperts, R. L. Martin, D. J. Fox, T. Keith, M. A. Al-Laham, C. Y. Peng, A. Nanayakkara, C. Gonzalez, M. Challacombe, P. M. W. Gill, B. G. Johnson, W. Chen,

M. W. Wong, J. L. Andres, M. Head-Gordon, E. S. Replogle and J. A. Pople, *GAUSSIAN 98 (Revision A.9)*, Gaussian, Inc., Pittsburgh, PA, 1998.
61 A. P. Scott and L. Radom, *J. Phys. Chem.*, 1996, **100**, 16502–16513.



Looking for that **special** chemical science research paper?

TRY this free news service:

Chemical Science

- highlights of newsworthy and significant advances in chemical science from across RSC journals
- free online access
- updated daily
- free access to the original research paper from every online article
- also available as a free print supplement in selected RSC journals.*

*A separately issued print subscription is also available.

Registered Charity Number: 207890

20030682

RSCPublishing

www.rsc.org/chemicalscience